

## Electronic Supplementary Information

1

2

### 3 **GSH-depleting chemodynamic therapy agent with photothermal and** 4 **photoacoustic properties for tumor theranostics**

5 Feng Liu,<sup>acd</sup> Lin Lin,<sup>ad</sup> Shu Sheng,<sup>acd</sup> Caina Xu,<sup>ad</sup> Yanbing Wang,<sup>ade</sup> Ying Zhang,<sup>acd</sup> Dianwei Wang,<sup>ade</sup> Jiayan  
6 Wu,<sup>ade</sup> Yanhui Li,<sup>\*b</sup> Huayu Tian,<sup>\*acde</sup> and Xuesi Chen,<sup>acde</sup>

7 <sup>a</sup>. Key Laboratory of Polymer Ecomaterials, Changchun Institute of Applied Chemistry, Chinese Academy of Sciences, Changchun 130022,  
8 China

9 <sup>b</sup>. School of Materials Science and Engineering, Changchun University of Science and Technology, Changchun 130022, China

10 <sup>c</sup>. University of Chinese Academy of Sciences, Beijing 100049, China

11 <sup>d</sup>. Jilin Biomedical Polymers Engineering Laboratory, Changchun 130022, China

12 <sup>e</sup>. University of Science and Technology of China, Hefei 230026, China

13

## 14 Experimental procedures

15 **Chemicals and reagents:**  $\text{FeCl}_3 \cdot 6\text{H}_2\text{O}$  and 3,3',5,5'-tetramethylbenzidine (TMB) were purchased from J&K Chemicals (Beijing, China). 2,2'-  
16 azinobis (3-ethylbenzothiazoline-6-sulfonic acid) ammonium salt (ABTS), polyvinylpyrrolidone (PVP), methylene blue (MB), 1,10-  
17 phenanthroline monohydrate (Phe) and 5,5-dimethyl-1-pyrroline N-oxide (DMPO) were purchased from Aladin (Shanghai, China). 3-(4, 5-  
18 dimethylthiazol-2-yl)-2, 5-diphenyltetrazolium bromide (MTT) was purchased from Amresco. Dulbecco's modified Eagle's medium  
19 (DMEM) and fetal bovine serum (FBS) were purchased from Gibco (Grand Island, USA). ROS kit was purchased from Beyotime  
20 Biotechnology (Jiangsu, China). Reduced GSH assay kit was purchased from Nanjing Jiancheng Bioengineering Institute (Jiangsu, China).  
21 All the other chemicals were from Sinopharm Chemical reagent Co., Ltd. (China) without treatment.

22  
23 **Instruments:** Zeta potential and size of nanoparticles were measured by zeta potential/BI-90Plus particle size analyzer (Brookhaven).  
24 Scanning electron microscopy (SEM) image was gained by Model XL 30 ESEM scanning electronic microscope. UV-vis absorption spectra  
25 were recorded by UV-1700 Spectrophotometer. Fourier-transform infrared spectroscopy (FTIR) spectra were obtained from Nicolet 520  
26 FTIR spectrometer. Powder X-ray diffraction (PXRD) spectrum was characterized by a  $\text{D}_8$  ADVANCE X-ray diffractometer (40 kV and  
27 40 mA). X-ray photoelectron spectroscopy (XPS) spectrum was characterized by ESCALab220i-XL electron spectrometer at a power of  
28 300 W Al  $\text{K}\alpha$  radiations (VG Scientific). Elemental analysis was measured by VARIO EL-III Elemental Analyzer. The content of Fe element  
29 was detected by inductively coupled plasma mass spectroscopy (ICP-MS) (Thermo Scientific Xseries 2, Thermo Fisher Scientific, USA). The  
30 Brunauer-Emmett-Teller (BET) curves was measured by a Micromeritics ASAP 2010 analyzer. Electron paramagnetic resonance (EPR)  
31 results were characterized by Bruker ELEXSYS (Germany).

32 **Preparation of AFP NPs:** 120 mg of ABTS and 120 mg of  $\text{FeCl}_3 \cdot 6\text{H}_2\text{O}$  were added to 20 mL of methanol under vigorous shaking. After  
33 10 min, the solution was dropped into the aqueous solution of PVP (400 mg, 80 mL). After vigorous stirring for 20 min at room  
34 temperature, the suspension mixture was purified by repetitive sequence (3 times) of centrifugation (8, 000 rpm, 5 min), and  
35 redispersion was then dried under vacuum.

36  
37 **Stability:** The stability of AFP NPs was investigated by monitoring the size of AFP NPs in cell culture medium and FBS at different time  
38 points.

39  
40 **Photothermal effect of AFP NPs:** The influence of AFP NPs concentration on photothermal effect was investigated by varying the AFP  
41 NPs concentration under the same radiation condition ( $1.0 \text{ W/cm}^2$ , 10 min). The influence of power density was also evaluated by  
42 recording the temperature of AFP NPs aqueous solution ( $100 \mu\text{g/mL}$ ) under the 808 nm laser with different power density. Besides, the  
43  $\text{H}_2\text{O}_2$  and acid enhanced photothermal effect were investigated in different concentrations of  $\text{H}_2\text{O}_2$  (0, 50 and  $100 \mu\text{M}$ ) and pH (5.0, 6.5  
44 and 7.4) by varying the AFP NPs concentration under the same irradiation condition ( $1.0 \text{ W/cm}^2$ , 10 min).

45  
46 **Photostability of AFP NPs:** AFP NPs solution ( $100 \mu\text{g/mL}$ ) was irradiated with laser (808 nm,  $1.0 \text{ W/cm}^2$ , 7 min) and then turned off the  
47 laser, leaving the solutions natural cooling for 5 min. The process was repeated for four times.

48  
49 **PAI capability of AFP NPs:** For  $\text{H}_2\text{O}_2$  enhanced PAI, PAI signal of AFP NPs solutions with different concentrations in the presence of  $\text{H}_2\text{O}_2$   
50 (0, 50 and  $100 \mu\text{M}$ ) was recorded by MSOT scanner (MSOT in Vision 128, iThera Medical GmbH, Germany). For acid enhanced PAI, the  
51 PAI signal of AFP NPs solutions with different concentrations in different pH (5.0, 6.5 and 7.4) was recorded.

52  
53 **Hydroxyl radical ( $\bullet\text{OH}$ ) generation ability of AFP NPs:** Electron paramagnetic resonance was utilized to investigated to the generation of  
54  $\bullet\text{OH}$  by employing 5,5-dimethyl-1-pyrroline N-oxide (DMPO) as a trapping probe. Besides, the generation of  $\bullet\text{OH}$  was also investigated  
55 through monitoring the absorption change of TMB and MB by UV-vis spectra. Briefly, the solution of 0.2 mM TMB or  $10 \mu\text{g/mL}$  MB

56 treated with different formulations was incubated at 37 °C for 2 h, then the •OH-induced TMB or MB oxidation was monitored by the  
57 absorbance intensity change at 665 nm.

58

59 **GSH-depletion ability of AFP NPs:** GSH-depletion ability of AFP NPs was first investigated by UV-vis spectra. To investigate the reduction  
60 of Fe<sup>3+</sup> in the presence of GSH, the absorbance intensity change at 525 nm in the presence of Phe was recorded. Besides, the absorbance  
61 intensity alteration at 425 nm of AFP NPs solution in the presence of GSH (10 mM) was also monitored to evaluate the GSH-depletion  
62 ability of oxidized ABTS (oxABTS). Further, quantitative results of GSH-depletion capability of AFP NPs was analyzed by reduced GSH kit.

63

64 **Cell uptake:** Cell uptake effect was investigated by evaluating the amount of Fe in cell treated with AFP NPs for different duration. Briefly,  
65 4T1 cells were seeded in 12 well plates (1×10<sup>5</sup>/well). After 24 h of incubation, cells treated with AFP NPs for different period were  
66 washed with PBS for three times. Then the cells were placed into -20 °C after introducing cell lysis buffer into every well. Then the  
67 solution of every well was collected to detect amount of Fe by ICP-MS after 24 h.

68

69 **Cytotoxicity assay:** The cytotoxicity of AFP NPs was evaluated through MTT assay. Briefly, 4T1 cells were seeded in 96-well plates at the  
70 density of 8000 cells/well and cultured for 24 h (37 °C, 5% CO<sub>2</sub>). After treated with AFP NPs with different concentrations, the plates  
71 were incubated for another 24 h. Subsequently, MTT (20 μL, 5 mg/mL) was introduced to each well, the medium was totally removed  
72 and 150 μL DMSO was added to each well after another 4 h of incubation. The cytotoxicity was measured by using a Bio-Read microplate  
73 reader at 492 nm.

74

75 **Intracellular reactive oxygen species (ROS) assay:** 4T1 cells were seeded in 12-well plates (1×10<sup>5</sup>/well). After 24 h incubation, cells were  
76 treated with different formulations for 12 h. Then cells were washed with PBS to remove before stained with ROS kit for 30 min.  
77 Subsequently, the intracellular DCF fluorescence was observed by using fluorescence microscope.

78

79 **Mouse tumor model:** Female BALB/C mice of 4 or 5-week old were purchased from Vital River Company in Beijing. All animal  
80 experiments were observed the guidelines for laboratory animals established by the Animal Care and Use Committee of Northeast  
81 Normal University. To establish the 4T1 tumor model, 2×10<sup>6</sup> cells in PBS (100 μL) were implanted into the right flank of each mouse by  
82 subcutaneous injection. When the tumor volume reached needed volume, *in vivo* experiments were then conducted.

83

84 **Photoacoustic imaging *in vivo*:** 4T1 tumor-bearing mice intravenously injected with AFP NPs (10 mg/kg, 0.2 mL) were imaged by PAI  
85 equipment at different time points. The wavelength in the scanning process was set at 680, 730, 760, 800, 850 and 900 nm. The scanning  
86 results were reconstructed at a by linear model and analyzed by linear regression.

87

88 **Thermal imaging *in vivo*:** 4T1 tumor-bearing mice were injected with PBS and AFP NPs, respectively. After 2 h, the tumor region of mice  
89 was irradiated with an 808 nm laser (1.0 W/cm<sup>2</sup>, 10 min), and the temperature of tumor site was imaged by an infrared camera.

90

91 **Antitumor therapeutic efficacy *in vivo*:** 4T1 tumor-bearing mice were randomly split into four groups (n = 5 per group), PBS, Fe<sup>3+</sup>, AFP  
92 and AFP/L group. The tumors were injected with different formulations (50 μL) in all corresponding groups (Fe<sup>3+</sup> group: injected with Fe<sup>3+</sup>  
93 at the dose of 2.4 mg/kg; AFP and AFP/L groups, injected with AFP NPs at the dose of 10 mg/kg). The tumors of AFP/L group were  
94 irradiated with the 808 nm NIR laser for 10 min at power density of 1.0 W/cm<sup>2</sup> after injected with AFP NPs for 2 h. The mice of all the  
95 groups were injected intratumorally with different formulations every two day, tumor volume and the body weight and were monitored  
96 every two day. Tumor volume was calculated by the formula:  $A \times B^2 / 2$  (A represents longer diameter and B represents the shorter). After  
97 14 days of treatments, the mice were sacrificed, major organs and the tumors were collected for further H&E analysis.

98

---

99 **Statistical analysis:** All measurements were conducted in triplicate, mean value and standard deviation (mean  $\pm$  SD) were calculated and  
100 displayed for all the data. The statistical analysis of different groups was compared through Student's t-test (\* $p < 0.05$  was considered  
101 statistically significant. \*\* $p < 0.01$  and \*\*\* $p < 0.001$  were considered extremely significant).

102

103

104 **Results and discussion**

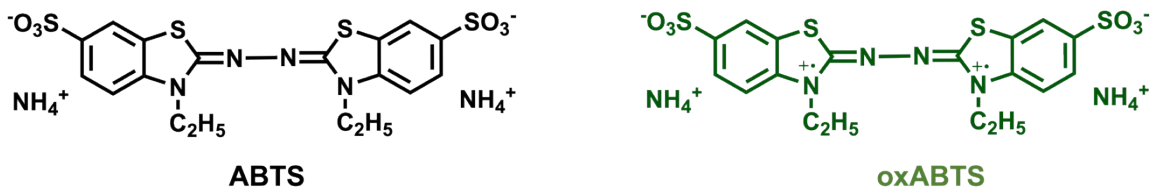


Figure S1. Molecular structure of ABTS and oxidized ABTS (oxABTS).

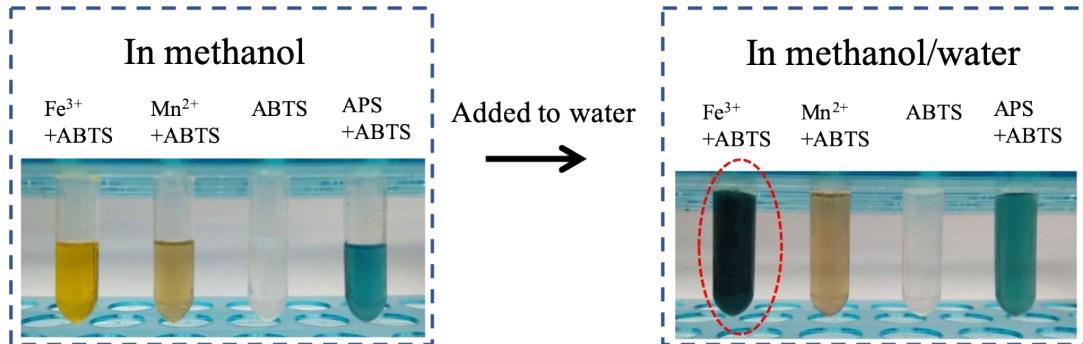


Figure S2. Photograph of solutions in methanol and methanol/water.

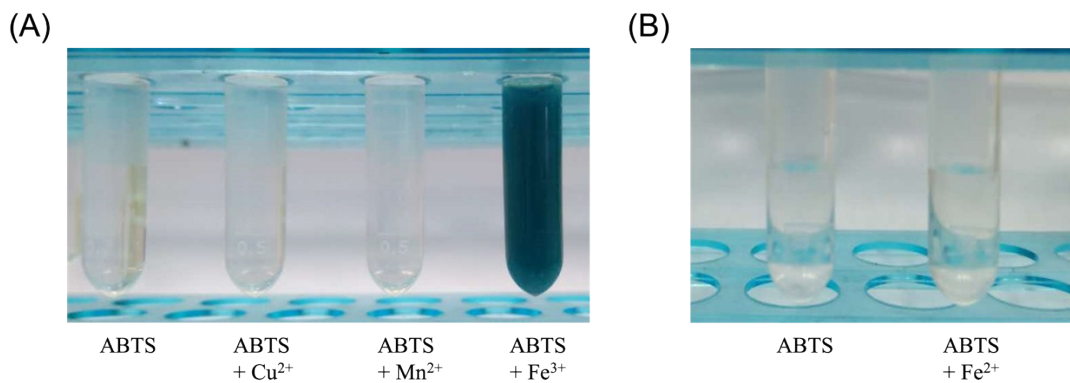


Figure S3. Photograph of solutions in water.

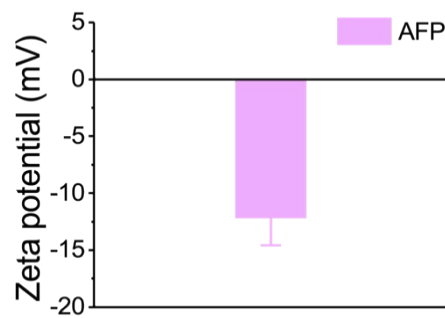


Figure S4. Zeta potential of AFP NPs.

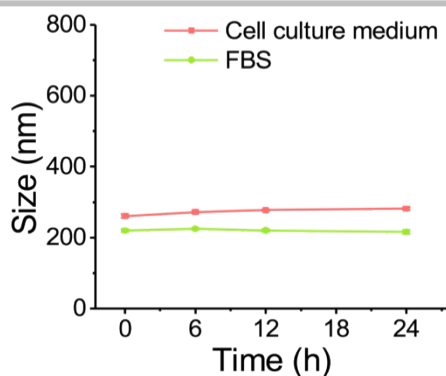


Figure S5. Stability of AFP NPs in DMEM cell culture medium and FBS.

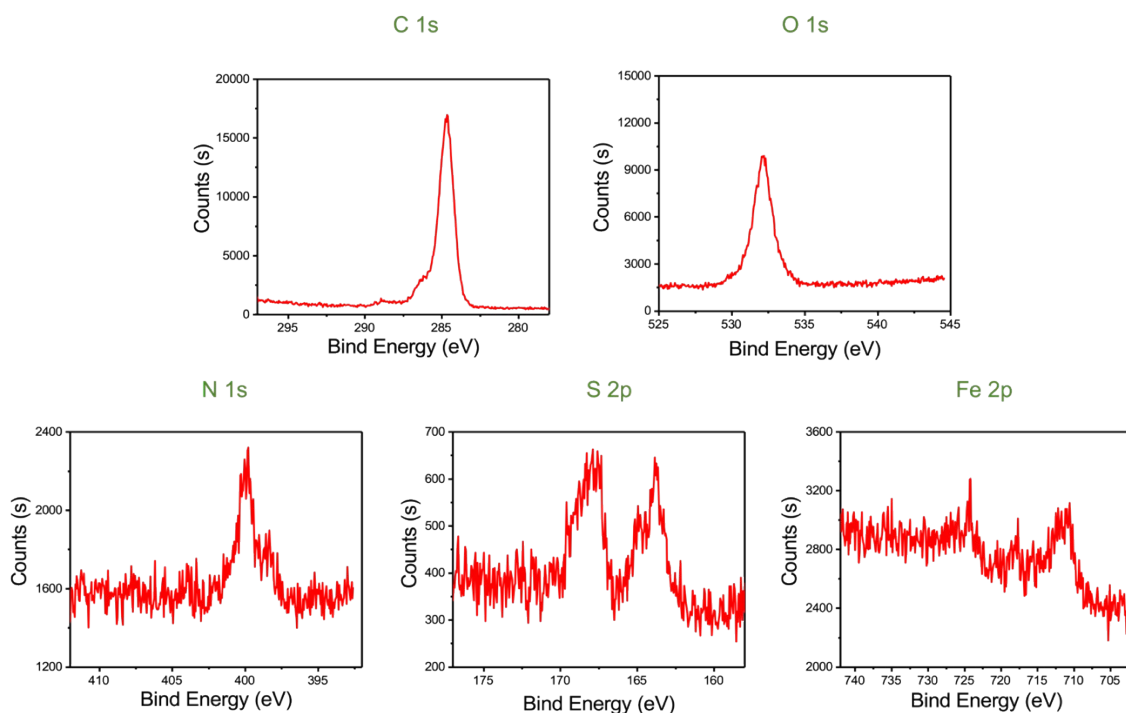
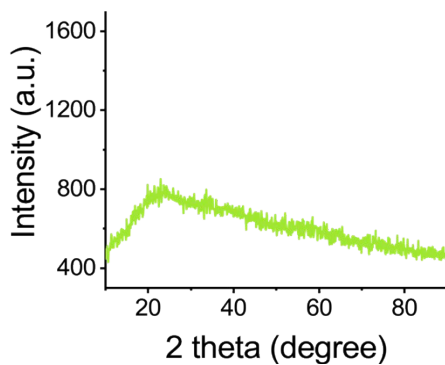


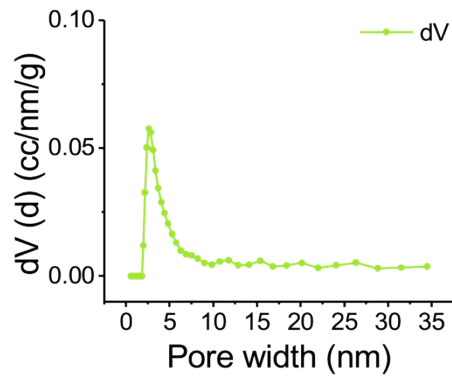
Figure S6. XPS spectra of C 1s, O 1s, N 1s, S 2p and Fe 2p of AFP NPs.

The characteristic peaks at 167.6 eV and 163.8 eV assigned to  $2p_{3/2}$  and  $2p_{1/2}$  of S were observed in Figure S3, confirming the presence of ABTS in AFP NPs.<sup>[1]</sup> Besides, the characteristic peaks at 710.6 eV and 724.2 eV can be assigned to  $2p_{3/2}$  and  $2p_{1/2}$  of Fe, demonstrating the presence of Fe in AFP NPs.<sup>[2]</sup>



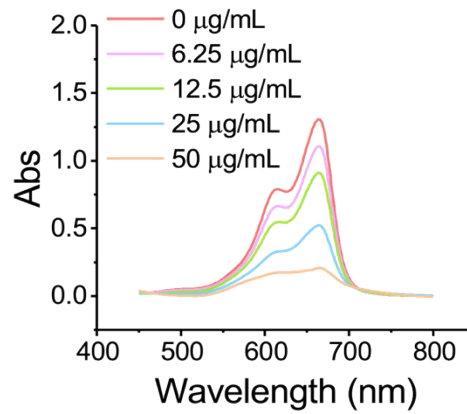
124  
125

Figure S7. XRD result of AFP NPs.



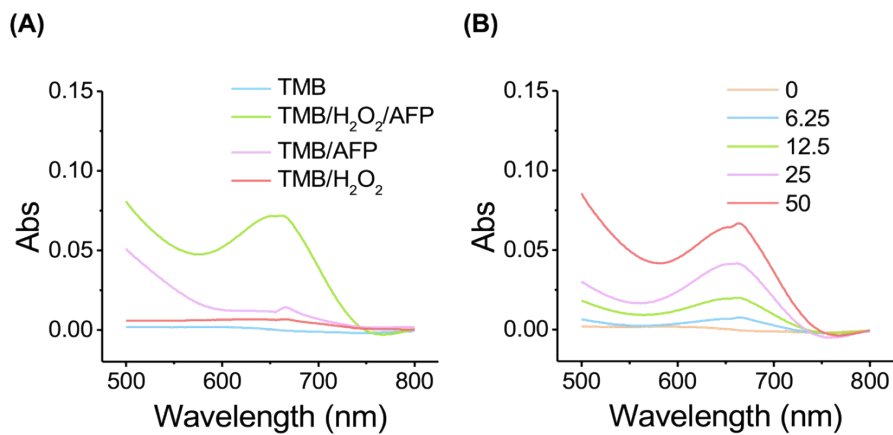
126  
127  
128

Figure S8. Pore size of AFP NPs.



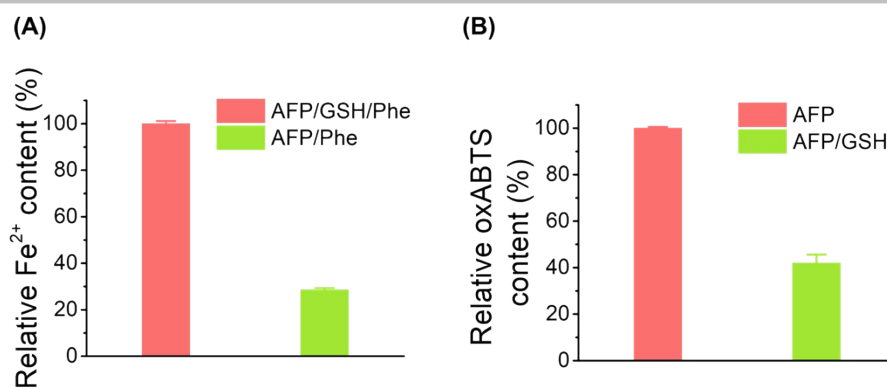
129  
130  
131

Figure S9. UV-vis absorption spectra of MB treated with AFP NPs of different concentrations in the presence of H<sub>2</sub>O<sub>2</sub> (100 μM).



132  
133  
134  
135

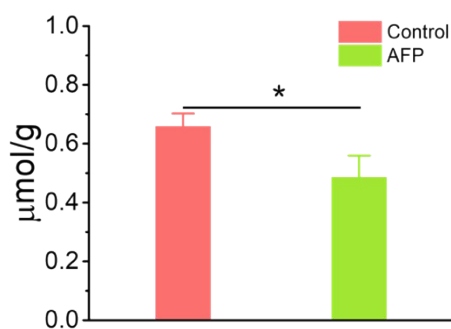
Figure S10. (A) UV-vis absorption spectra of TMB solution treated with different groups. (B) UV-vis absorption spectra of TMB treated with different concentrations of AFP NPs in the presence of 100 μM H<sub>2</sub>O<sub>2</sub>.



136

137 **Figure S11.** (A) Relative Fe<sup>2+</sup> content in the solution of AFP/Phe and AFP/GSH/Phe calculated from Figure 2D. (B) Relative oxABTS content  
 138 in the solution of AFP and AFP/GSH calculated from Figure 2C.

139

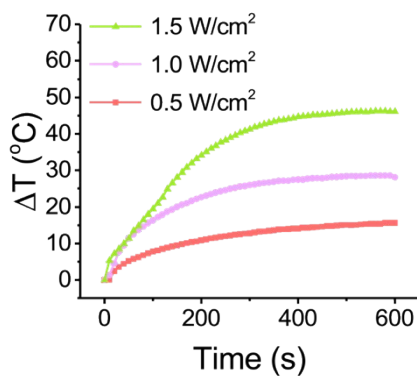


140

141 **Figure S12.** The GSH level of non-treated tumor and the tumor injected with AFP NPs for 24 h (n = 3).  
 142

141

142

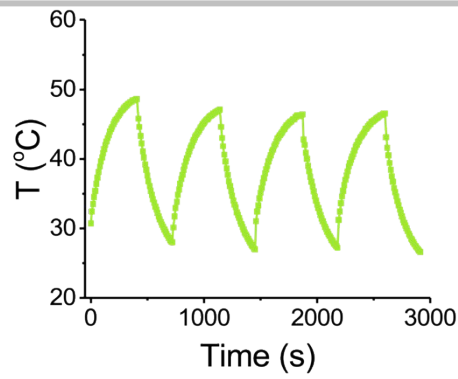


143

144 **Figure S13.** Temperature curves of AFP NPs irradiated with laser of different power density.  
 145

144

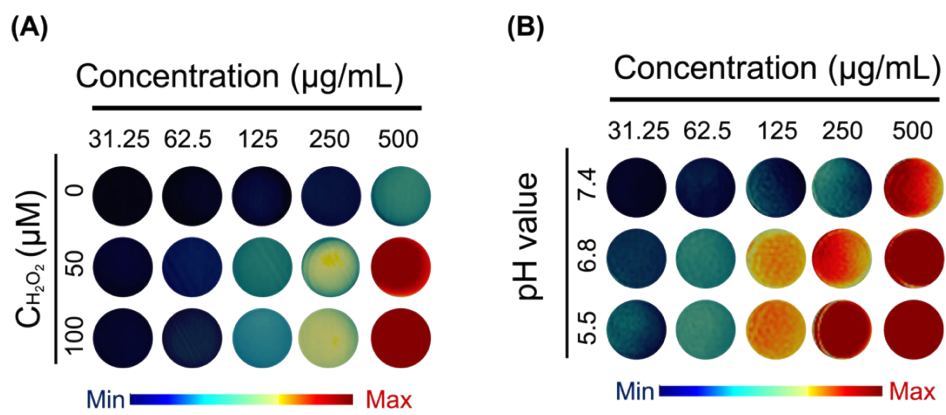
145



146

147 **Figure S14.** Temperature curve of AFP NPs solution after four cycles of heating and cooling. In this experiment, AFP NPs aqueous solution  
 148 was irradiated with laser (808 nm, 1.0 W/cm<sup>2</sup>, 7 min) and then shut off (5 min). The process was repeated for four cycles.

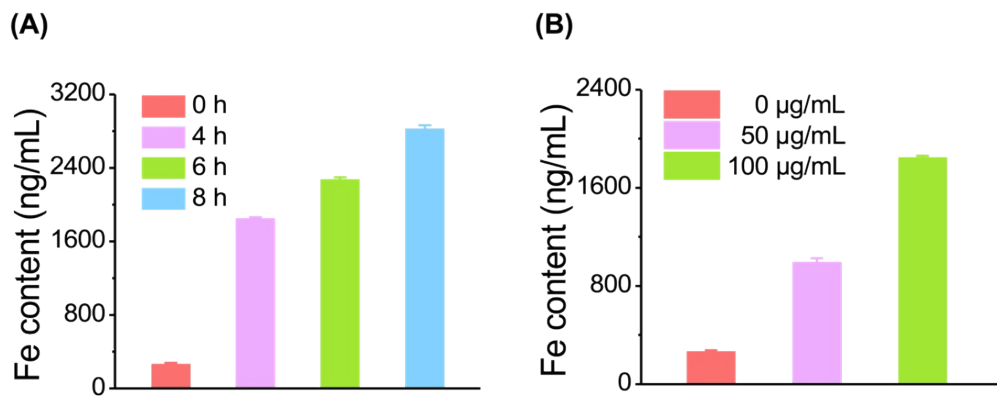
149



150

151 **Figure S15.** PAI images of AFP NPs solution in (A) H<sub>2</sub>O<sub>2</sub> with different concentrations and (B) buffer with different pH values.

152



153

154 **Figure S16.** (A) The quantitative analysis of Fe content in 4T1 cells after treated with AFP NPs at different time points (n = 3). (B) The  
 155 quantitative analysis of Fe content in 4T1 cells treated with AFP NPs with different concentrations after 4 h of incubation.

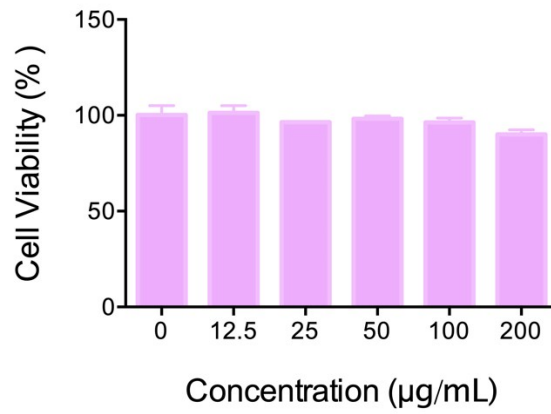


Figure S17. Cytotoxicity of AFP NPs with different concentration to 4T1 cells.

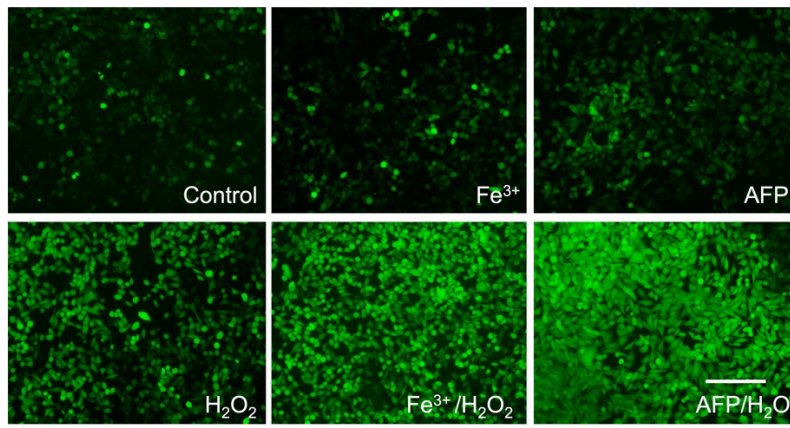


Figure S18. ROS level of 4T1 cells treated with different formulations (scale bar is 200 µm).

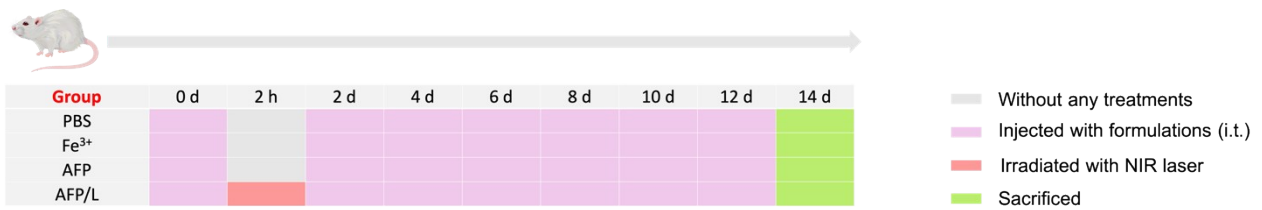
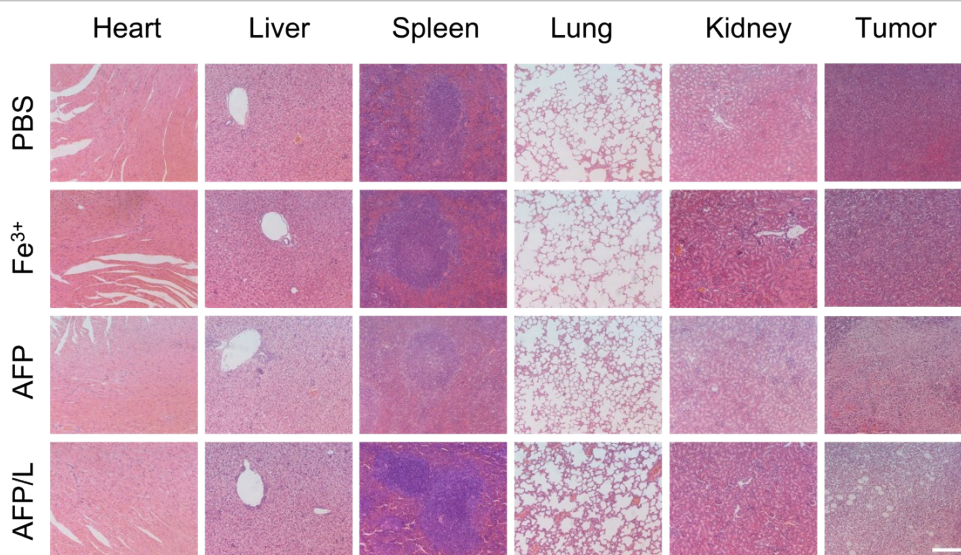


Figure S19. Treatment schedule of different groups.



**Figure S20.** H&E staining images of the major organs of treated mice at 14 days post-treatment (scale bar is 200  $\mu$ m).

**Table S1.** Element analysis of AFP NPs.

N (%)	C (%)	H (%)	S (%)
5.99	24.35	4.12	10.54

**Table S2.** ICP-MS result of AFP NPs.

Element	wt%
Fe	23.8

165

166

167

168

169

170

171

172

## 173 References

174 1 G. Li, J. Sun, W. Hou, S. Jiang, Y. Huang, J. Geng, *Nat. Commun.* 2016, **7**, 10601.

175 2 T. Yamashita, P. Hayes, *Appl. Surf. Sci.* 2008, **254**, 2441-2449.

176